Paper Number: **51**

Title: **Implementation of a Tabulated Failure Model Into a Generalized Composite Material Model Suitable for Use in Impact Problems**

Authors (names are for example only): Robert K. Goldberg
Kelly S. Carney
Paul DuBois
Canio Hoffarth
Bilal Khaled
Loukham Shyamsunder
Subramaniam Rajan
Gunther Blankenhorn

(FIRST PAGE OF ARTICLE – *align this to the top of page – leave space blank above ABSTRACT*)

ABSTRACT

The need for accurate material models to simulate the deformation, damage and failure of polymer matrix composites under impact conditions is becoming critical as these materials are gaining increased use in the aerospace and automotive communities. The aerospace community has identified several key capabilities which are currently lacking in the available material models in commercial transient dynamic finite element codes. To attempt to improve the predictive capability of composite impact simulations, a next generation material model is being developed for incorporation within the commercial transient dynamic finite element code LS-DYNA. The material model, which incorporates plasticity, damage and failure, utilizes experimentally based tabulated input to define the evolution of plasticity and damage and the initiation of failure as opposed to specifying discrete input parameters such as modulus and strength. The plasticity portion of the orthotropic, three-dimensional, macroscopic composite constitutive model is based on an extension of the Tsai-Wu composite failure model into a generalized yield function with a non-associative flow rule. For the damage model, a strain equivalent formulation is used to allow for the uncoupling of the deformation and damage analyses. For the failure model, a tabulated approach is utilized in which a stress or strain based invariant is defined as a function of the location of the current stress state in stress space to define the initiation of failure. Failure surfaces can be defined with any arbitrary shape, unlike traditional failure models where the mathematical functions used to define the failure surface impose a specific shape on the failure surface. In the current paper, the complete development of the failure model is described and the generation of a tabulated failure surface for a representative composite material is discussed.

Robert K. Goldberg, NASA Glenn, 21000 Brookpark Road, Cleveland, OH 44135
Kelly S. Carney, George Mason University, 4400 University Drive, Fairfax, VA 22030
Paul DuBois, George Mason University, 4400 University Drive, Fairfax, VA 22030
Canio Hoffarth, Arizona State University, 1151 S. Forest Avenue, Tempe, AZ, 85287
Bilal Khaled, Arizona State University, 1151 S. Forest Avenue, Tempe, AZ 85287
Loukham Shyamsunder, Arizona State University, 1151 S. Forest Avenue, Tempe, AX 85287
Subramaniam Rajan, Arizona State University, 1151 S. Forest Avenue, Tempe, AZ, 85287
Gunther Blankenhorn, Livermore Software Technology Corporation, 7374 Los Positas Road, Livermore, CA 94551

INTRODUCTION

As composite materials are gaining increased use in aircraft components where impact resistance is critical (such as the turbine engine fan case), the need for accurate material models to simulate the deformation, damage and failure response of polymer matrix composites under impact conditions is gaining in importance. While there are several material models currently available within commercial transient dynamic codes such as LS-DYNA [1] to analyze the impact response of composites, areas have been identified where the predictive capabilities of these models can be improved. These limitations have been extensively discussed in Goldberg, et al [2, 3]. Of particular relevance to the current study, one major limitation of the currently existing models is that the input to these models generally consists of point-wise properties (such as the modulus, failure stress or failure strain in a particular coordinate direction) that leads to curve fit approximations to the material stress-strain curves and simplified approximations to the actual material failure surfaces. This type of approach either leads to models with only a few parameters, which provide a crude approximation at best to the actual material response, or to models with many parameters which require a large number of complex tests to characterize. An improved approach is to use tabulated data, obtained from well-defined set of straightforward experiments. Using tabulated data allows the actual material response data to be entered in a discretized form, which permits a more accurate representation of the actual material response.

To begin to address these limitations in the currently existing models, a new composite material model incorporating deformation, damage and failure is being developed and implemented for use within LS-DYNA. The material model is meant to be a fully generalized model suitable for use with a large number of composite architectures (laminated or textile). The deformation model, described extensively in Goldberg, et al [2], is based on extending the commonly used Tsai-Wu composite failure model [4] to a strain hardening plasticity model with a non-associative flow rule. For the damage model, described extensively in Goldberg, et al [3], a strain equivalent formulation is used in which the deformation and damage calculations can be uncoupled. A significant feature in the developed damage model is that a semi-coupled approach has been utilized in which a load in a particular coordinate direction results in damage (and thus stiffness reduction) in multiple coordinate directions. This semi-coupled approach, while different from the methodology used in many existing damage mechanics models [3], has the potential to more accurately reflect the damage behavior that actually takes place, particularly for composites with more complex fiber architectures.

A wide variety of failure models, which mark the end of the stress-strain curve, have been developed for composites. In models such as the Tsai-Wu failure model [4], a quadratic function of the macroscopic stresses is defined in which the coefficients of the failure function are related to the tensile, compressive and shear failure stresses in the various coordinate directions. This model, while mathematically simple and easy to implement numerically, assumes that the composite failure surface has an ellipsoidal (in 2D) or ovoid (in 3D) shape. In reality, composite failure surfaces often are not in the form of simple shapes. More complex models, such as the Hashin model [5], also utilize quadratic combinations of the macroscopic failure stresses, but utilize only selective terms in the quadratic function in order to link the macroscopic

stresses to local failure modes such as fiber or matrix failure. However, an overall quadratic form to the failure functions (albeit in a piecewise fashion) are still assumed. This approach was extended in models such as those developed by Puck et al. [6], Pinho et al. [7] and Maimi et al. [8], in which complex equations were developed to predict local failure mechanisms in terms of macroscopic level stresses. In this manner, the failure response and complex failure surfaces present in actual composites could be more accurately represented. However, in these advanced models, very complex tests are often required to characterize the model parameters and the applicability of the models may be limited to specific composite architectures with specific failure mechanisms. In a combination of approaches, researchers such as Mayes and Hansen [9] and Feng [10] utilize an approach where stress (or strain) invariants based on macroscopic stresses are used to define the initiation of failure. However, different forms of the invariants are used to determine whether fiber-dominated or matrix-dominated failure occurs. Given the variety of failure models present in the literature, activities such as the World Wide Failure Exercise and its multiple iterations (e.g. [11], [12], and [13]) have attempted to conduct a rigorous review of which failure model or models provides the optimum prediction of composite failure. In all of these studies, none of the examined models showed a complete ability to predict composite failure or displayed a significant advantage compared to the other models examined.

The difficulty in simulating composite failure can be related to the fact that in reality failure is a highly localized phenomenon dependent on various combination of fiber, matrix and interface failures. Due to these complex and interacting local failure mechanisms, and the fact that these mechanisms can vary based on the constituent materials and fiber architecture, in reality the actual composite failure surface often does not conform to a shape that can be easily simulated using a simple mathematical function. Conversely, attempts to utilize discrete functions to analyze the complex local mechanisms can result in models with a large number of parameters that require a highly complex test program to obtain. In the methodology described in this paper, an approach is used in which the actual experimental three-dimensional failure envelope for a composite is entered in a tabulated fashion. Specifically, a stress or strain based invariant leading to the initiation of failure is defined as a function of the location of the current stress state in stress space. In this manner, an arbitrary failure surface can be easily defined based on actual experimental data in combination with numerical data obtained using any desired existing failure model. The current approach thus serves as a general framework which is not limited to any arbitrarily imposed failure surface based on an arbitrarily defined mathematical function.

In the following sections of this paper, a brief summary of the deformation and damage models are presented. Details of the failure model are then discussed, including the overall methodology along with its application for a representative composite material.

DEFORMATION MODEL OVERVIEW

A complete description of the deformation model is given in Goldberg et al [2]. A summary of the key features of the model is presented here. In the deformation model, a general quadratic three-dimensional orthotropic yield function based on the

Tsai-Wu failure model is specified as follows, where 1, 2, and 3 refer to the principal material directions

$$f(\sigma) = -1 + \begin{pmatrix} F_1 & F_2 & F_3 & 0 & 0 & 0 \end{pmatrix} \begin{pmatrix} \sigma_{11} \\ \sigma_{22} \\ \sigma_{33} \\ \sigma_{12} \\ \sigma_{23} \\ \sigma_{31} \end{pmatrix} + \begin{pmatrix} \sigma_{11} & \sigma_{22} & \sigma_{33} & \sigma_{12} & \sigma_{23} & \sigma_{31} \end{pmatrix} \begin{pmatrix} F_{11} & F_{12} & F_{13} & 0 & 0 & 0 \\ F_{12} & F_{22} & F_{23} & 0 & 0 & 0 \\ F_{13} & F_{23} & F_{33} & 0 & 0 & 0 \\ 0 & 0 & 0 & F_{44} & 0 & 0 \\ 0 & 0 & 0 & 0 & F_{55} & 0 \\ 0 & 0 & 0 & 0 & 0 & F_{66} \end{pmatrix} \begin{pmatrix} \sigma_{11} \\ \sigma_{22} \\ \sigma_{33} \\ \sigma_{12} \\ \sigma_{23} \\ \sigma_{31} \end{pmatrix} \quad (1)$$

In the yield function, σ_{ij} represents the stresses and F_{ij} and F_k are coefficients that vary based on the current values of the yield stresses in the various coordinate directions. By allowing the coefficients to vary, the yield surface evolution and hardening in each of the material directions can be precisely defined. The values of the normal and shear coefficients can be determined by simplifying the yield function for the case of unidirectional tensile and compressive loading in each of the coordinate directions along with shear tests in each of the shear directions. In the above equation, the stresses are the current value of the yield stresses in the normal and shear directions. To determine the values of the off-axis coefficients (which are required to capture the stress interaction effects), the results from 45° off-axis tests in the various coordinate directions can be used. The values of the off-diagonal terms in the yield function can also be modified as required in order to ensure that the yield surface is convex [2].

A non-associative flow rule is used to compute the evolution of the components of plastic strain. The plastic potential for the flow rule is shown below

$$h = \sqrt{H_{11}\sigma_{11}^2 + H_{22}\sigma_{22}^2 + H_{33}\sigma_{33}^2 + 2H_{12}\sigma_{11}\sigma_{22} + 2H_{23}\sigma_{22}\sigma_{33} + 2H_{31}\sigma_{33}\sigma_{11} + H_{44}\sigma_{12}^2 + H_{55}\sigma_{23}^2 + H_{66}\sigma_{31}^2} \quad (2)$$

where σij are the current values of the stresses and H_{ij} are independent coefficients, which are assumed to remain constant. The values of the coefficients are computed based on average plastic Poisson's ratios [2]. The plastic potential function in Equation (2) is used in a flow law to compute the components of the plastic strain rate, where the usual normality hypothesis from classical plasticity [14] is assumed to apply and the variable $\dot{\lambda}$ is a scalar plastic multiplier.

$$\dot{\boldsymbol{\varepsilon}}^p = \dot{\lambda} \frac{\partial h}{\partial \boldsymbol{\sigma}} \quad (3)$$

Given the flow law, the principal of the equivalence of plastic work [14] can be used to determine that the plastic potential function h can be defined as the effective stress and the plastic multiplier can be defined as the effective plastic strain rate.

To compute the current value of the yield stresses needed for the yield function, in the developed model tabulated stress-strain curves are used to track the yield stress evolution. The user is required to input twelve stress versus plastic strain curves. Specifically, the required curves include uniaxial tension curves in each of the normal directions (1,2,3), uniaxial compression curves in each of the normal directions (1,2,3), shear stress-strain curves in each of the shear directions (1-2, 2-3 and 3-1), and 45 degree off-axis tension curves in each of the 1-2, 2-3 and 3-1 planes. The 45 degree curves are required in order to properly capture the stress interaction effects. By utilizing tabulated stress-strain curves to track the evolution of the deformation response, the experimental stress-strain response of the material can be captured exactly without any curve fit approximations. The required stress-strain data can be obtained either from actual experimental test results or by appropriate numerical experiments utilizing stand-alone codes. Currently, only static test data is considered. Future efforts will involve adding strain rate and temperature dependent effects to the computations. To track the evolution of the deformation response along each of the stress-strain curves, the effective plastic strain is chosen to be the tracking parameter. Using a numerical procedure based on the radial return method [14] in combination with an iterative approach, the effective plastic strain is computed for each time/load step. The stresses for each of the tabulated input curves corresponding to the current value of the effective plastic strain are then used to compute the yield function coefficients.

DAMAGE MODEL OVERVIEW

The deformation portion of the material model provides the majority of the capability of the model to simulate the nonlinear stress-strain response of the composite. However, in order to capture the nonlinear unloading and local softening of the stress-strain response often observed in composites [15], a complementary damage law is required. In the damage law formulation, strain equivalence is assumed, in which for every time step the total, elastic and plastic strains in the actual and effective stress spaces are the same [16]. The utilization of strain equivalence permits the plasticity and damage calculations to be uncoupled, as all of the plasticity computations can take place in the effective stress space.

The first step in the development of the damage model is to relate the actual stresses to a set of effective stresses by use of a damage tensor **M**

$$\boldsymbol{\sigma} = \mathbf{M}\boldsymbol{\sigma}_{eff} \tag{4}$$

The effective stress rate tensor can be related to the total and plastic strain rate tensors by use of the standard elasto-plastic constitutive equation

$$\dot{\boldsymbol{\sigma}}_{eff} = \mathbf{C}\left(\dot{\boldsymbol{\varepsilon}} - \dot{\boldsymbol{\varepsilon}}_{p}\right) \tag{5}$$

where **C** is the standard elastic stiffness matrix and the actual total and plastic strain rate tensors are used due to the strain equivalence assumption.

In order to maintain a one to one relationship between the effective stresses and the actual stresses (i.e. to ensure that a uniaxial load in the actual stress space does not result in a multi-axial load in the effective stress space), the damage tensor is assumed to be diagonal, leading to the following form (assuming the stresses are written in vector form).

$$[\mathbf{M}] = \begin{bmatrix} M_{11} & 0 & 0 & 0 & 0 & 0 \\ 0 & M_{22} & 0 & 0 & 0 & 0 \\ 0 & 0 & M_{33} & 0 & 0 & 0 \\ 0 & 0 & 0 & M_{44} & 0 & 0 \\ 0 & 0 & 0 & 0 & M_{55} & 0 \\ 0 & 0 & 0 & 0 & 0 & M_{66} \end{bmatrix} \tag{6}$$

An implication of a diagonal damage tensor is that loading the composite in a particular coordinate direction only leads to a stiffness reduction in the direction of the load due to the formation of matrix cracks perpendicular to the direction of the load. However, as discussed in detail in Goldberg, et al [3], in actual composites, particularly those with complex fiber architectures, a load in one coordinate direction can lead to stiffness reductions in multiple coordinate directions. To maintain a diagonal damage tensor while still allowing for the damage interaction in at least a semi-coupled sense, each term in the diagonal damage matrix should be a function of the plastic strains in each of the normal and shear coordinate directions. Note that plastic strains are chosen as the "tracking parameter" due to the fact that, within the context of the developed formulation, the material nonlinearity during loading is simulated by use of a plasticity based model. The plastic strains therefore track the current state of load and deformation in the material.

To explain this concept of damage coupling further, assume a load is applied in the 1 direction to an undamaged specimen. The undamaged modulus in the 1 direction is E_{11} and the undamaged modulus in the 2 direction is E_{22}. The stress-strain response of the material is assumed to become nonlinear (represented in the current model by the accumulation of plastic strain) and damage is assumed to occur. The original specimen is unloaded and reloaded elastically in the 1 direction. Due to the damage, the reloaded specimen has a reduced modulus in the 1 direction of E_{11}^{d11}. The reduced modulus is a function of the damage induced by the loading and the resulting nonlinear deformation in the 1 direction (reflected as plastic strain), where d_{11}^{11} is the damage in the 1 direction due to a load in the 1 direction. Alternatively, if the damaged specimen was reloaded elastically in the 2 direction, due to the assumed damage coupling resulting from the load in the 1 direction, the reloaded specimen would have a reduced modulus in the 2 direction of E_{22}^{d11}. The reduced modulus is a function of the damage induced by the load and resulting nonlinear deformation in the 1 direction, where d_{11}^{22} is the damage in the 2 direction due to a load in the 1 direction.

Similar arguments can be made and equations developed for the situation where the original specimen is loaded in the 2 direction.

For the case of multiaxial loading, the semi-coupled formulation needs to account for the fact that as the load is applied in a particular coordinate direction, the loads are acting on damaged areas due to the loads in the other coordinate directions, and the load in a particular direction is just adding to the damaged area. For example, if one loaded the material in the 2 direction first, the reduced modulus in the 1 direction would be equal to E_{11}^{d22}. If one would then subsequently load the material in the 1 direction, the baseline modulus in the 1 direction would not be equal to the original modulus E_{11}, but instead the reduced modulus E_{11}^{d22}. Therefore, the loading in the 1 direction would result in the following further reduction in the modulus in the 1 direction:

$$E_{11}^{d11} = \left(1 - d_{11}^{11}\left(\varepsilon_{11}^{p}\right)\right)E_{11}^{d22} = \left(1 - d_{11}^{11}\left(\varepsilon_{11}^{p}\right)\right)\left(1 - d_{22}^{11}\left(\varepsilon_{22}^{p}\right)\right)E_{11} \tag{7}$$

These results can be extended to suggest that the relation between the actual stress and the effective stress should be based on a multiplicative combination of the damage terms as opposed to an additive combination of the damage terms.

To properly characterize the damage model in a tabulated fashion, each of the damage parameters has to be determined as a function of the plastic strain in a particular coordinate direction. For example, to determine the damage terms for the case of loading in the 1 direction, a composite specimen has to be loaded to a certain plastic strain level in the 1 direction. The material is then unloaded to a state of zero stress, and then reloaded elastically in each of the coordinate directions to determine the reduced modulus of the material in each of the coordinate directions. This data can then be used to determine the values of the damage parameters for a particular value of plastic strain. This process then needs to be repeated for multiple values of plastic strain to determine a full tabulated characterization of the damage parameters as a function of plastic strain.

FAILURE MODEL

As discussed earlier in this paper, the majority of the available failure models utilize mathematical functions to describe the failure surface, which impose a specific shape on the failure surface. An example of this concept can be seen in Figure 1. In this figure, a two-dimensional failure surface in the σ_{11}-σ_{22} plane for the case of zero shear stresses generated using the two-dimensional version of the classical Tsai-Wu failure model for a representative AS4/3501-6 polymer matrix composite is shown. The properties used to generate the failure surface were taken from Daniel and Ishai [4] and are listed in Table 1. Note that the actual failure surface is continuous but slight discontinuities are shown in the presented graphs due to numerical issues in the generation of the graph. As can be seen in the figure, the failure surface is elliptical due to the quadratic nature of the equation defining the failure surface. In reality, however, as shown for example in some of the cases discussed by Daniel and Ishai [4], the failure surfaces of actual composites often do not exhibit this simple shape. Many actual failure surfaces cannot be easily defined by a mathematical function of

the stresses. Alternatively, as shown in Figure 1, one potential method of defining the points in the failure surface is to use a cylindrical type of coordinate system. In this approach, a variable θ defines the relative location of the point on the failure surface in stress space, while a second variable r defines the "magnitude" of the failure surface point in the stress space location. Since the relationship between "r" and "θ" also cannot be easily defined by a mathematical function for a realistic composite failure surface, a tabulated approach, where a series of "r" and "θ" pairs are explicitly defined for a given failure surface, can provide a more accurate representation of the failure surface. Buyak [17] has demonstrated that tabulated approaches can be successful in defining complex failure surfaces for advanced materials based on experimental data. The tabulated approach allows for the use of experimentally defined failure surface data, a failure surface defined using any existing failure model, or a combination of experimental and numerically obtained "virtual" data. The combined approach can allow for the case where actual failure data are only available for a portion of the total stress space, with "virtual" data being required to fill in the gaps in the failure surface.

Independent and Dependent Variables

As described above, for the tabulated failure surface definition proposed in this study appropriate independent and dependent variables need to be defined. The independent variables need to define the location of a point on the failure surface in stress space, and the dependent variable needs to define the magnitude of the failure surface point along the lines defined by the independent variables. For the current approach, the in-plane and out-of-plane responses will be considered separately. First, the definition of the in-plane failure surface will be discussed. For the in-plane failure surface definition, two independent variables are defined. The first independent variable will be the ratio of the shear stress to the shear failure stress. For selected values of this shear ratio, the location of each defined point on the failure surface in stress space is specified by defining the angle of the point in the σ_{11}-σ_{22} plane, as shown in Figure 1, which becomes the second independent variable. Using simple geometric principals, the angle θ for each defined point on the failure surface can be defined in terms of the stresses σ_{11} and σ_{22} as shown below. To ensure a set of unique, monotonically increasing angles from -180° to 180°, if the stress σ_{22} is negative the computed angle is multiplied by -1 as shown below:

$$\theta = \cos^{-1}\left(\frac{\sigma_{11}}{\sqrt{\sigma_{11}^2 + \sigma_{22}^2}}\right) \qquad (8)$$
$$\theta_{act} = -\theta \; if \; \sigma_{22} \leq 0$$

For the dependent variable, which is used to define the magnitude of the failure surface point given a particular location in stress space, a stress invariant first identified by Fleischer [18] is used, defined as follows for the plane stress case:

$$r = \sqrt{\sigma_{11}^2 + \sigma_{22}^2 + 2\sigma_{12}^2} \qquad (9)$$

This invariant can be considered to be like a "radius" from the origin to the failure surface. The factor of 2 in front of the shear stress term reflects the symmetry of the stress tensor. Stresses or strains can be used in defining the dependent variable, making the model more general. Using an invariant type of term also allows for the stress interactions to be more appropriately accounted for in the failure definition and helps to ensure that the failure definition will be accurate for a variety of loading conditions. One difficulty in using a tabulated approach of this type is that for many polymer matrix composites the failure surface is highly anisotropic due to the high failure strength in the fiber direction and the much lower failure stresses in the transverse direction. If one were to scale the y axis of the graph shown in Figure 1 such that it was equal to the scale of the x axis, one would observe that the actual failure surface is highly elongated. Due to the significant elongation of the failure surface, if one were to plot the radius versus the angle for the failure surface defined above, the majority of the points of the failure surface would be clustered at angles near -180°, 0°, and 180°. This clustering would create round-off and interpolation difficulties in the numerical implementation of the failure model, making the current definition undesirable.

To facilitate a more even distribution of the tabulated failure surface points along the entire spectrum of angles, the stresses used in the definition of the independent variable θ can be scaled. For the current method, the stresses in the 11-direction are arbitrarily scaled by the longitudinal tensile failure stress, and the 22-direction stresses are scaled by the transverse tensile failure stress. Revised angles are then computed using these scaled stresses. The value of the dependent variable *r*, however, is still computed using the actual unscaled stresses. A plot of the radius versus the angle computed using the scaled stresses is shown in Figure 2. As can be seen in this figure, the points defining the failure surface are fairly evenly distributed along the range of angles. Having evenly distributed points will allow for much smoother and more accurate interpolations when used in a numerical implementation.

Modified Center of Failure Surface

As mentioned earlier, for the proposed approach the procedure described above needs to be repeated for several ratios of the shear stress to the shear failure stress in order to fully define the in-plane failure surface. As failure surfaces similar to that shown in Figure 1 are generated with higher shear stress values, one can observe that increasing the shear stresses results in a failure surface with the same shape as the surface generated assuming zero shear stresses, but the location of the failure surface is shifted somewhat towards the negative stress quadrant of the graph. At high values of shear stresses, the failure surface may not even include the origin. Even when the origin is included, the fact that the failure surface is not centered on the origin may cause the angle calculations to be skewed. If the failure surface does not include the origin, the angle calculations would not even be valid as they would not be unique.

To mitigate this issue, in the current approach the origin of the scaled failure surfaces for the selected shear stress ratios are redefined such that they lie in the center of the failure surface. The modified center of each failure surface is then defined based on the maximum and minimum scaled stress values in the 11- and 22-directions as shown below. Modified stresses in the 11- and 22-directions are then defined in terms of the modified center as shown below:

$$\sigma_{11-center} = \frac{1}{2}\left(\sigma_{11-\max} + \sigma_{11-\min}\right)$$
$$\sigma_{22-center} = \frac{1}{2}\left(\sigma_{22-\max} + \sigma_{22-\min}\right) \quad (10)$$
$$\sigma_{11-\mathrm{mod}} = \sigma_{11} - \sigma_{11-center}$$
$$\sigma_{22-\mathrm{mod}} = \sigma_{22} - \sigma_{22-center}$$

The angle calculations shown in Equation (8) are carried out using the revised stresses. The radius calculations are carried out using the original, unscaled and unmodified stresses. An example of the modified, scaled, re-centered failure surface for the case of zero shear stresses is shown in Figure 3. As can be observed in the figure, the overall shape of the failure surface does not change from the original case but the failure surface is now centered about the modified origin. The radius versus scaled angle plot determined using the modified failure surface center is shown in Figure 4. As can be seen in the figure, the tabulated points defining the failure surface are more evenly distributed compared to the case with the original origin location shown in Figure 2.

Algorithm for Implementation of In-Plane Failure Model

To apply the in-plane version of the failure model described above, first the failure surface for a given composite needs to be converted into a tabulated form in order to establish a benchmark for determining if failure has occurred for a given load condition. The baseline failure surface for a given material can be established based on experimental data, any available numerical failure model, or a combination of the two. In the combination approach, experimental data can be used where available, and analytically generated data can be used to fill in the required gaps. Given the baseline failure surface data, Equations (8)-(10) are then used to generate a series of "radius" versus "angle" plots for various ratios of shear stress to shear failure stress, similar to Figure 4. For use in a numerical algorithm, the data needs to be transformed into a set of tables which serve as input to the computer model. The stress values defining the "center" of the failure surface for the selected shear stress ratios also need to be defined for use in the calculations.

The specific algorithm to implement the failure model is as follows:

1.) Given: applied load condition σ_{11}, σ_{22}, σ_{12}.

2.) Compute the shear ratio $R = \sigma_{12}/S$.

3.) Scale the longitudinal and transverse stresses.

4.) Look up the appropriate modified failure surface center stresses ($\sigma_{11\text{-center}}$ and $\sigma_{22\text{-center}}$) (Equation (4)) corresponding to the current shear ratio R. Note that interpolation of these stresses may be required if the current shear ratio R is not explicitly defined in the input tables.

5.) Compute the modified longitudinal and transverse stresses given the stresses defining the modified failure surface center.

6.) Compute the angle θ associated with the modified longitudinal and transverse stresses.

7.) Compute the radius associated with the unscaled, unmodified applied stresses.

8.) Compare the radius computed at step 7) to the tabulated radius at failure for the given shear ratio R and angle θ. Note that interpolation of the radius at failure may be required if the specific values of R and θ are not specified in the input tables.

9.) If the radius computed using the applied stresses is equal to or greater than the radius at failure, the material is assumed to have failed. In the numerical implementation, the element will either be eroded once failure is deemed to have occurred or have all of its stiffness properties reduced to negligible values. A progressive reduction in stresses will not occur.

Algorithm for Implementation of In-Plane Failure Model

The methodology and procedures described above are valid for the case of in-plane loading and stresses. For thin composites, particularly under in-plane loading, this case is most likely sufficient since the out-of-plane normal and transverse shear stresses can be assumed to be negligible. However, for thicker composites, particularly under impact loading conditions, the out-of-plane stresses can often be significant and must be included. One way to account for failure due to out-of-plane stresses is to utilize a delamination model, as is discussed in many sources such as Barbero [15]. In this case, the in-plane failure model could be used in combination with a delamination model to fully define the composite failure. However, an alternative approach would be to define a tabulated failure surface defined by the out-of-plane stresses that is independent from the failure surface defined by the in-plane stresses. The radius-like dependent variable can then be used to couple the failure responses due to the in-plane and out-of-plane stresses.

The out-of-plane failure surface can be defined in a manner similar to what was used to define the in-plane failure surface. To generate the required out-of-plane failure surfaces, a series of two dimensional failure surfaces in the σ_{13}-σ_{23} plane are defined for various ratios of the out-of-plane normal stress σ_{33} to the out-of-plane normal failure stress. Equations similar to Equations (8) and (10) can then be used to define the values of the angle θ (where σ_{11} in the equations is replaced with σ_{13} and σ_{22} in the equations is replaced with σ_{23}) for the out-of-plane failure surfaces. For the dependent variable, a stress invariant radius term similar to Equation (9) is defined:

$$r = \sqrt{\sigma_{33}^2 + 2\sigma_{13}^2 + 2\sigma_{23}^2} \tag{11}$$

where the transverse shear stresses are multiplied by 2 due to the symmetry of the stress tensor. Plots of the radius versus scaled angle (similar to those shown in Figure 4) can then be generated for several out-of-plane normal stress ratios based on the out-of-plane failure stresses and converted into a tabulated set of input for the failure model.

For the case where both in-plane and out-of-plane stresses are present in a material under a specified load state, a method needs to be specified to allow for the stress interactions that may take place under the combination of in-plane and out-of-plane loading. To account for the stress interaction, ratios d_{ip} and a ratio d_{oop} are defined. The ratio d_{ip} represents the ratio of the radius computed using Equation (9) for the applied in-plane stresses to the corresponding radius computed using the in-plane stresses at failure for a given angle and shear stress ratio. The ratio d_{oop}

represents the ratio of the radius computed using Equation (11) for the applied out-of-plane stresses to the radius at failure for a given out-of-plane angle and out-of-plane normal stress ratio. A weighted sum of the ratios can then be computed using the following expression, where n is an arbitrary number defined by the user:

$$d = \sqrt[n]{d_{ip}^{n} + d_{oop}^{n}} \tag{12}$$

If the weighted ratio *d* is greater than or equal to one, failure is assumed to have occurred. If the weighted ratio *d* is less than one, failure is assumed to have not occurred.

CONCLUSIONS

A generalized composite model suitable for use in polymer composite impact simulations has been developed. The model utilizes a plasticity based deformation model obtained by generalizing the Tsai-Wu failure criteria. A strain equivalent damage model has also been developed in which loading the material in a particular loading direction can lead to damage in multiple coordinate directions. A general, tabulated failure model has also been formulated. Within the failure model, a methodology has been developed to convert two-dimensional failure surfaces to a tabulated format based on the location of the points of the failure surface in stress space and a dependent stress invariant variable which defines the magnitude of the failure stress points at a given location. An algorithm to implement the failure model has been developed, and a procedure for accounting for a combination of in-plane and out-of-plane stresses has been specified.

ACKNOWLEDGEMENTS

Authors Hoffarth, Khaled, Shyamsunder and Rajan gratefully acknowledge the support of (a) the Federal Aviation Administration through Grant #12-G-001 titled "Composite Material Model for Impact Analysis", William Emmerling, Technical Monitor, and (b) NASA through Contract Number: NN15CA32C titled "Development and Implementation of an Orthotropic Plasticity Progressive Damage Model for Transient Dynamic/Impact Finite Element Analysis of Composite Structures", Robert Goldberg, Contracting Officer Representative.

REFERENCES

1. Hallquist, J. 2013. *LS-DYNA Keyword User's Manual, Version 970*. Livermore Software Technology Corporation, Livermore, CA.
2. Goldberg, R., K. Carney, P. DuBois, C. Hoffarth, J. Harrington, S. Rajan, and G. Blankenhorn. 2015. "Development of an Orthotropic Elasto-Plastic Generalized Composite Material Model Suitable for Impact Problems," *Journal of Aerospace Engineering*, 29:04015083.
3. Goldberg, R., K. Carney, P. DuBois, C. Hoffarth, S. Rajan, and G. Blankenhorn. 2015. "Incorporation of Plasticity and Damage Into an Orthrotropic Three-Dimensional Model With Tabulated Input Suitable for Use in Composite Impact Problems," NASA/TM-2015-218849, National Aeronautics and Space Administration, Washington, D.C.
4. Daniel, I.M., and O. Ishai. 2006. *Engineering Mechanics of Composite Materials Second Edition*. Oxford University Press, New York.

5. Hashin, Z. 1980. "Failure Criteria for Unidirectional Fiber Composites," *Journal of Applied Mechanics*, 47:329-334.
6. Puck, A., and H. Schurmann. 1998. "Failure Analysis of FRP Laminates by Means of Physically Based Phenomenological Models," *Composites Science and Technology*, 58:1045–1067.
7. Pinho, S.T., L. Iannucci, and P. Robinson. 2006. "Physically-Based Failure Models and Criteria for Laminated Fibre-Reinforced Composites With Emphasis on Fibre Kinking: Part I: Development," *Composites: Part A*, 37:63-73.
8. Maimi, P., P.P. Camanho, J.A. Mayugo, and C.G. Davila. 2007. "A Continuum Damage Model for Composite Laminates: Part I-Constitutive Model," *Mechanics of Materials*, 39:897-908.
9. Mayes, J.S., and A.C. Hansen. 2001. "Multicontinuum Failure Analysis of Composite Structural Laminates," *Mechanics of Composite Materials and Structures*, 8:249-262.
10. Feng, W.W. 1991. "A Failure Criterion for Composite Materials," *Journal of Composite Materials*, 25:88-100.
11. Hinton, M.J., and A.S. Kaddour. 2012. "The background to the Second World-Wide Failure Exercise," *Journal of Composite Materials*, 46:2283-2294.
12. Kaddour, A.S., M.J. Hinton, P.A. Smith and S. Lee. 2013. "The background to the third world-wide failure exercise," *Journal of Composite Materials*, 47:2417-2426.
13. Kaddour, A.S., M.J. Hinton, P.A. Smith and S. Lee. 2013. "A comparison between the predictive capability of matrix cracking, damage and failure criteria for fibre reinforced composite laminates: Part A of the third world-wide failure exercise," *Journal of Composite Materials*, 47:2749-2779.
14. Khan, A.S., and S. Huang. 1995. *Continuum Theory of Plasticity*. John Wiley and Sons, New York.
15. Barbero, E.J. 2013. *Finite Element Analysis of Composite Materials Using ABAQUS*. CRC Press, Boca Raton, FL.
16. Lemaitre, J., and R. Desmorat. 2005. *Engineering Damage Mechanics: Ductile, Creep and Brittle Failures*. Springer, Berlin.
17. Buyak, M. 2014. "Development of a New Metal Material Model in LS-DYNA Part 2: Development of A Tabulated Thermo-Viscoplastic Material Model With Regularized Failure for Dynamic Ductile Failure Prediction of Structures Under Impact Loading," DOT/FAA/TC-13/25, P2, Federal Aviation Administration, Washington, D.C.
18. Fleischer M., T. Borrvall, and K.-U. Bletzinger. 2007. "Experience from using recently implemented enhancements for Material 36 in LS-DYNA 971 performing a virtual tensile test", *6th European LS-DYNA Users Conference*, Gothenburg, Sweden.

TABLE I. MATERIAL PROPERTIES FOR AS4/3501-6 UNIDIRECTIONAL COMPOSITE

Property	**Value**
Longitudinal Modulus E_{11} (GPa)	147
Transverse Modulus E_{22} (GPa)	10.3
Longitudinal Poisson's Ratio ν_{12}	0.27
Transverse Poisson's Ratio ν_{23}	0.54
In-Plane Shear Modulus G_{12} (GPa)	7.0
Longitudinal Tensile Strength X_T (MPa)	2280
Longitudinal Compressive Strength X_C (MPa)	1725
Transverse Tensile Strength Y_T (MPa)	57
Transverse Compressive Strength Y_C (MPa)	228
In-Plane Shear Strength S (MPa)	76

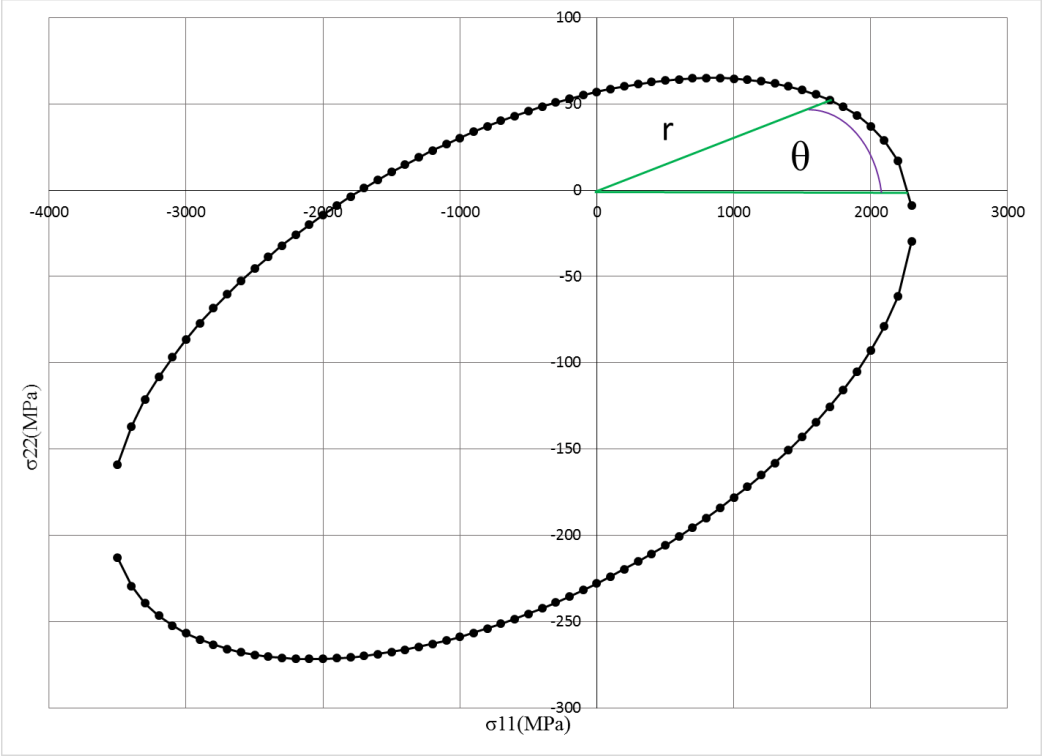

Figure 1. Tsai-Wu failure surface for AS4/3501-6 composite.

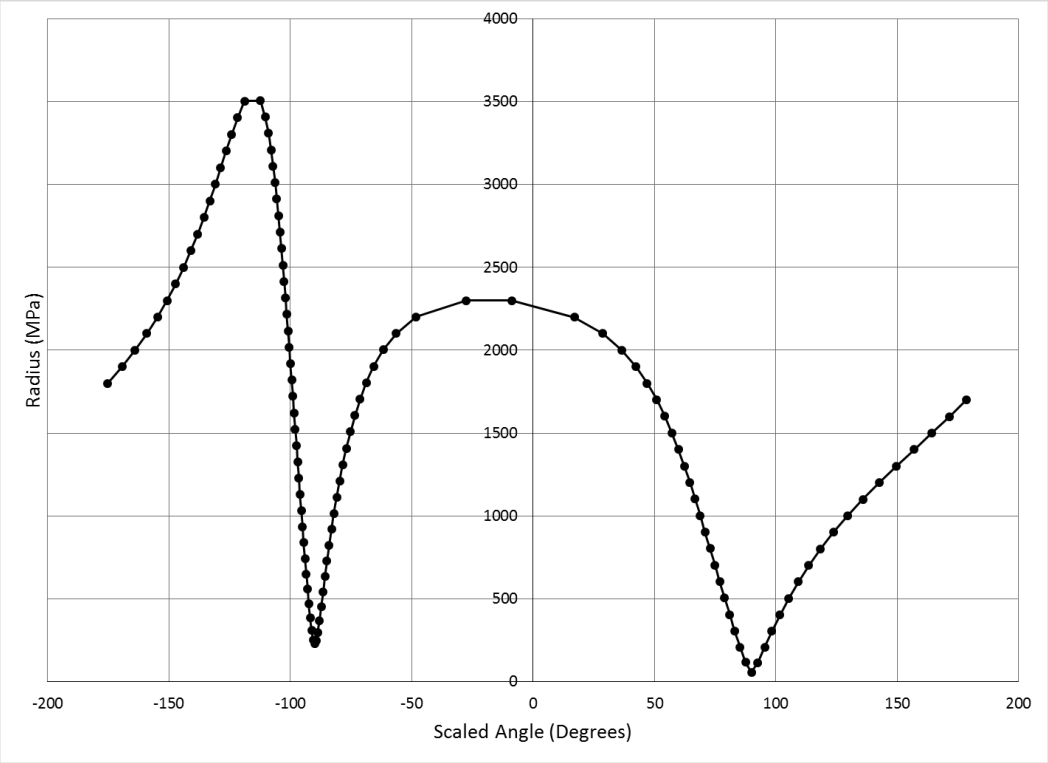

Figure 2. Plot of radius versus angle for scaled AS4/3501-6 failure surface.

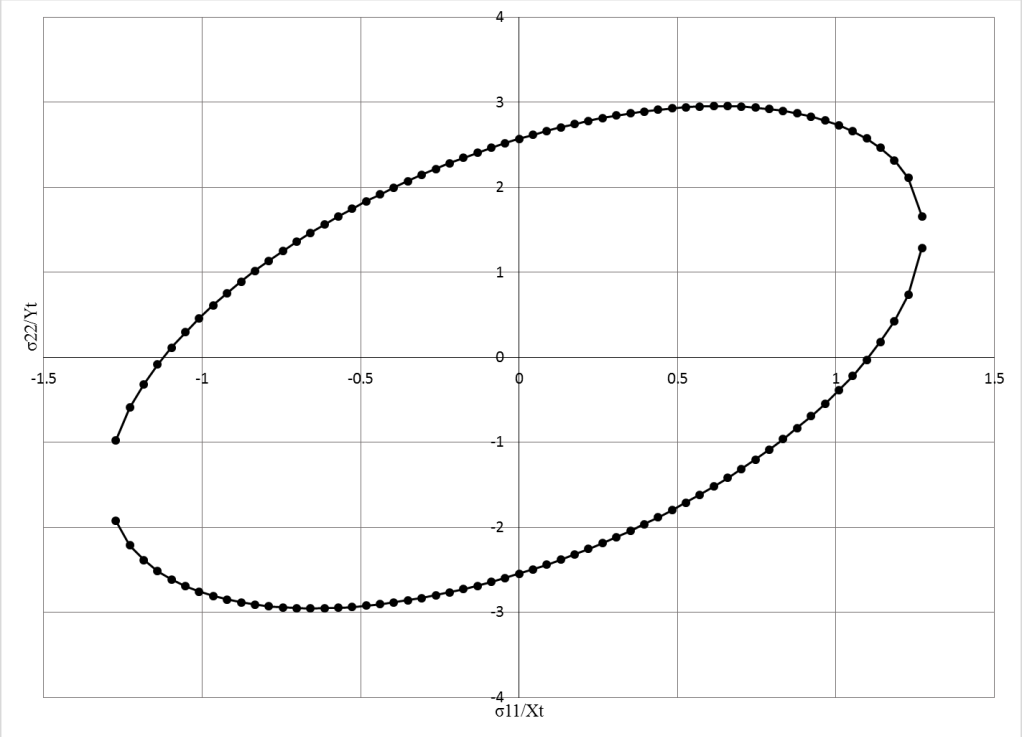

Figure 3. Scaled Tsai-Wu failure surface with modified center for AS4/3501-6 composite.

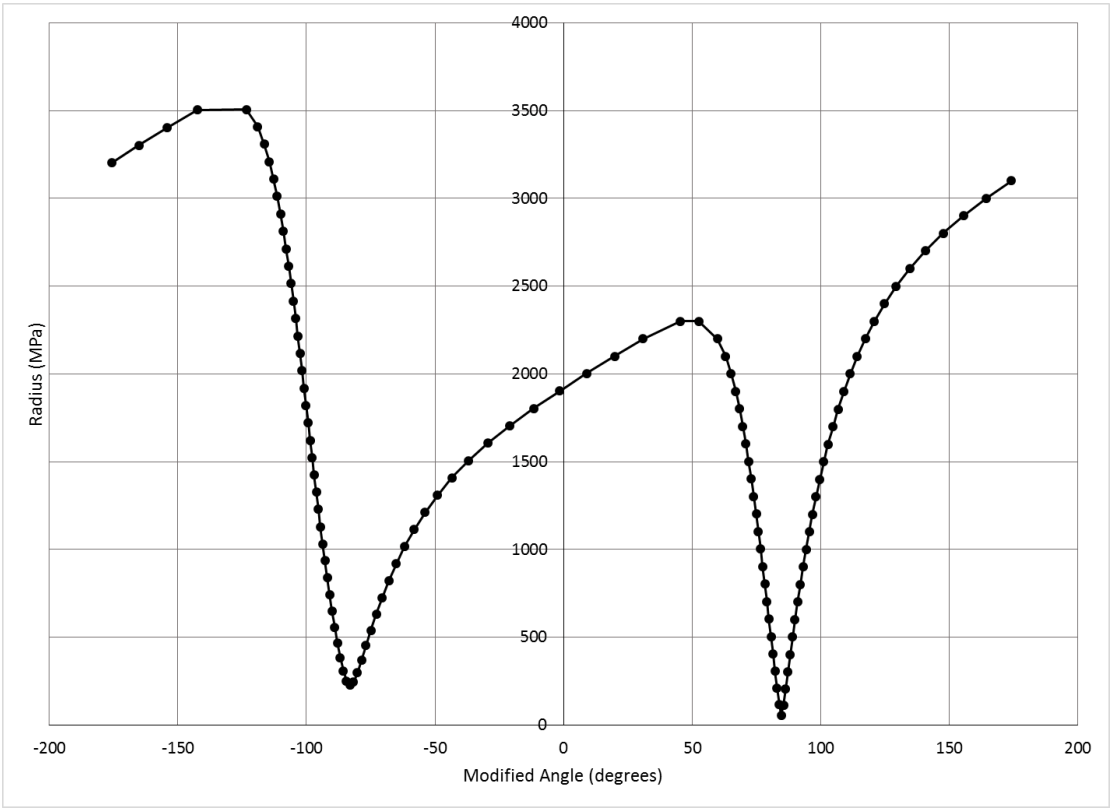

Figure 4. Plot of radius versus angle for scaled failure surface with modified center.